

Direct observation of strong t-e orbital hybridization and the effects of f orbitals

Mian Wang, Qian Zhang, Shuai Jing, Xiang-Guo Li,* and Yanglong Hou

School of Materials, Sun Yat-sen University, Shenzhen 518107, China

(Dated: March 13, 2024)

Recent research has revealed that the Cr family perovskite ReCrO_3 exhibits intriguing magnetic coupling interactions within Cr pairs, which may not follow the Goodenough-Kanamori (GK) rules due to the t-e hybridization between Cr^{III} ions. We investigate the complex magnetism involving both t-e hybridization and Re- f orbitals in the molecular analogue of perovskite $[\text{Ce}_2^{\text{III}}\text{Ce}^{\text{IV}}\text{Cr}_8^{\text{III}}\text{O}_8(\text{O}_2\text{CPh})_{18}(\text{HO}_2\text{CPh})]$ (Ce_3Cr_8) using first-principles method. Our results have shown that distinct from the bulk ReCrO_3 , the superexchange via Cr- d and O- p orbitals can exhibit an unexpected dominant ferromagnetic (FM) Cr-O-Cr superexchange interaction in Ce_3Cr_8 due to the strong t-e hybridization originated from the distorted molecular structure. The great sensitivity of the t-e hybridization with respect to the molecular structure, e.g., the angle of Cr-O-Cr, can lead to a ground state transition from ferromagnetic to antiferromagnetic state with the changes in the angle of Cr-O-Cr. The Ce- f orbitals near the Fermi level can reduce this sensitivity through interacting with the Cr- d orbitals via the virtual charge transfer process. Our results are strongly supported by a modified superexchange model based on the t-e hybridization theory. These findings complete the theory of superexchange magnetism involving the t-e hybridization and f orbitals, and in the meanwhile introduce a new avenue for fine-tuning the magnetic characteristics via Tm- d /Re- f interactions at nanoscale.

Magnetic perovskite materials continue to attract widespread attentions in the scientific community due to its excellent and fascinating physical properties such as colossal magnetoresistance and multiferroicity [1–7]. In particular, the chromium-based RECrO_3 (RE = rare earths) compounds show a broad application in the fields of catalyst, thermistor, fuel cell, and nonvolatile memory devices because of their intriguing magnetic and ferroelectric properties[8]. However, understanding the underlying magnetic exchange mechanisms still present great challenges due to its complexity. For example, a ferromagnetism (FM) from the t-e hybridization between Cr^{III} ions was reported previously in RECrO_3 [8–11], while the evidence is indirect and not adequate since the antiferromagnetic (AF) superexchange interaction is still the main contribution in the exchange path of $\text{Cr}^{\text{III}}\text{-O-Cr}^{\text{III}}$ with bridging angle much greater than 90° in bulk RECrO_3 , according to Goodenough-Kanamori rule[12–14]. The dominance of the FM superexchange interaction in such geometry, that is the direct evidence of the existence of t-e hybridization induced FM interaction, has never been achieved. Not to mention the quantitative analysis of this FM interaction.

The recently synthesized molecular analogue of the perovskite repeating unit $[\text{Ce}_2^{\text{III}}\text{Ce}^{\text{IV}}\text{Mn}_8^{\text{III}}\text{O}_8(\text{O}_2\text{CPh})_{18}(\text{HO}_2\text{CPh})]$, abbreviated as Ce_3Mn_8 , which manifests rich and complex physics with a variety of magnetic interactions involving f electrons[15], provides a new platform for the underlying exchange mechanism investigation. Introducing an extra d_σ electron by substituting Mn^{III} with Fe^{III} can result in more pronounced asymmetric behavior in the FM interaction involving transition metal (TM) 3d and

RE 4f orbitals [16]. Cr^{III} , on the other hand, without occupied d_σ orbitals can potentially exhibit more novel physics. For example, the more distorted molecular framework compared to its bulk counterpart may present a different degree/form of t-e hybridization. The RE- f orbitals can also potentially have significant effects on the t-e hybridization. Such physics have never been realized and investigated yet. In addition, the nanoscale size of the molecule enables the fine-tuning of its properties by chemical doping or external manipulation, which is intrinsically different from its corresponding bulk perovskite. Consequently, it is desirable to study these fundamental physics related to the magnetic exchange mechanisms in the molecular form of RE-Cr systems.

In this letter, we theoretically explore the complex magnetism in Ce_3Cr_8 , a molecular analogue of the perovskite repeating units by replacing Mn ions with Cr ions in Ce_3Mn_8 [15, 17], with main focus on the t-e hybridization and the effects of f orbitals using the first-principles method. Interestingly, our calculations show that FM exchange coupling between Cr ions via t-e hybridization is the dominant interaction in Ce_3Cr_8 leading to a FM ground state, distinct from its bulk RECrO_3 crystal in which AF interaction is still the leading interaction. The calculated exchange strengths at various Coulomb energies and Cr-O-Cr bond angles quantitatively agree with a simple model derived from orbital overlap integrations, further confirming the FM nature from t-e hybridization. More importantly, the Ce^{IV}- f orbital around the Fermi level can significantly change the sensitivity of strain induced exchange coupling changes through the virtual charge transfer between Ce-4f orbitals and Cr-3d orbitals, different from the direct FM contribution from f orbitals in Ce_3Mn_8 [15] and Ce_3Fe_8 [16] in our previous investigations. Our results add extra content for the fundamental superexchange coupling physics by directly demonstrating the dominant FM interaction in

* lixguo@mail.sysu.edu.cn

TM-O-TM with bonding angle much greater than 90° . The effects of f orbitals on such exchange mechanism can provide another dimension to modify and control the magnetic behavior in magnetic molecular-based devices.

Method.— Our first-principles calculations are carried out within the framework of Kohn-Sham Density Functional Theory (DFT) [18] with the generalized gradient corrected Perdew-Burke-Ernzerhof (PBE) exchange-correlation functional [19] using the Vienna Ab-initio Simulation Package (VASP) code [20, 21]. The electron-ion interaction was described using projector augmented wave (PAW) potentials [22, 23]. The energy cutoff for plane-wave basis expansion was set to 500 eV. The threshold for self-consistency and structure optimization were set to 10^{-5} eV and 0.01 eV/Å, respectively. The molecule was put into a large periodic supercell of $28 \text{ \AA} \times 22 \text{ \AA} \times 24 \text{ \AA}$ to make sure the distance between the molecule and its repeating image is larger than 10 Å. Because of the strong localization of Ce-*f* and Cr-*d* orbitals, the GGA+U method was applied with $U=2.0$ eV [15, 16, 24] and 3.0 eV [25] for the Ce-*f* and Cr-*d* orbitals, respectively. The Wannier90 package [26] was applied to calculate Wannier Functions. The spin-orbital coupling is switched off due to its negligible effects on the exchange coupling in 3d- and 4f-compounds [16, 27, 28].

Results.— The initial structure of Ce_3Cr_8 molecule is obtained by substituting Cr ions for Mn ions in the recently reported Ce_3Mn_8 molecule [15]. Analogy to $\text{Ce}_3\text{Mn}_8^{\text{III}}$, the $\text{Ce}_3\text{Cr}_8^{\text{III}}$ molecule have a striking structural similarity to the repeating unit of perovskite, which resembles a repeating unit of ABO_3 cubic with distortions and plus two A ions, as shown in Figure 1(a) and (b). The core of $\text{Ce}_3\text{Cr}_8^{\text{III}}$ includes eight Cr sites and three Ce sites. Three Ce ions are arranged in a line as shown in Fig. 1b. The central Ce ion has an oxidation state of +4 and is eight-coordinated, while the other two Ce ions have an oxidation state of +3 and are nine-coordinated. The eight Cr^{III} ions in $\text{Ce}_3\text{Cr}_8^{\text{III}}$ can be divided into two groups, each group has four Cr^{III} ions, which are separated by the Ce line, denoted as the top group (Cr1, Cr2, Cr3, Cr4) and the bottom group (Cr5, Cr6, Cr7, Cr8).

We perform the subsequent electronic structure calculations after a fully geometry optimization. We mainly focus on the nearest-neighbor (NN) exchange couplings of the Cr ions along the paths involving Cr-O-Cr geometries, including J_1 perpendicular to the Ce line (see Fig 1c) and J_2 parallel with the Ce line (see Fig 1d). In the neighboring CrO_6 of J_1 , the two Cr-O octahedras are edge-sharing with two bridging oxygen atoms with Cr-O-Cr bonding angles 110.8° and 90.5° , respectively (see Fig 1c); the neighboring CrO_6 within the J_2 share one corner with one bridging oxygen atom with Cr-O-Cr bonding angles 127.6° , and two carboxylate groups connect the two Cr ions within the neighboring CrO_6 octahedras (see Fig 1d).

The perovskite have four known common type of spin-ordering configurations: FM, A-AF, C-AF and G-AF [29]. While Ce_3Cr_8 molecule has low symmetry with three in-

equivalent interaction planes or axes along different orientations, leading to three distinct A-AF and three different C-AF states. Thus there are eight high symmetrical magnetic configurations (plus one G-AF and one FM) in Ce_3Cr_8 , illustrated in the supplementary Figure S1. Our results show that FM is the ground state of Ce_3Cr_8 molecule by performing DFT calculations for all eight magnetic configurations. The calculated total energies of these eight magnetic configurations are listed in Supplementary Table S1. The eight Cr ions in Ce_3Cr_8 have $2.8 \mu_B$ magnetic moment for each Cr which indicate an oxidation state of +3 [30]. The two Ce^{III} ions outside the Cr curb have a magnetic moments of $1 \mu_B$ for each, and the central Ce^{IV} has a small magnetic moments (less than $0.1 \mu_B$).

To reveal the underlying magnetic properties of Ce_3Cr_8 , the Cr/Cr exchange coupling parameters (J) are estimated by a multi-spin Heisenberg model [31–35] with total energies of different magnetic states. The spin Hamiltonian is defined as,

$$\hat{H} = - \sum_{i < j} J_{ij} \vec{s}_i \cdot \vec{s}_j \quad (1)$$

where J_{ij} are magnetic coupling parameters between the Cr ions at sites i and j ; \vec{s}_i and \vec{s}_j are the spin vectors of Cr ions at site i and j , respectively. The total spin of S is 1.5 for each Cr ion according to the Hund's rule. Our total energy results indicate that two spin coupling paths, J_1 to J_2 (see Fig. 1), exhibit significant contributions to the total energy. Other coupling paths, e.g., the diagonal direction of the side faces denoted as J_3 and J_4 , are shown in Supplementary Materials Fig. S1, which are much smaller compared to J_1 and J_2 (see Supplementary Material section I). The calculated coupling strengths (see Table I) are $J_1 = +1.09$ meV and $J_2 = +2.07$ meV (positive for FM, negative for AF). The strong FM interactions of J_1 and J_2 result in the FM ground state.

The dominant FM nature of J_1 and J_2 is unexpected after analysing the superexchange mechanisms. For example, in J_2 exchange coupling pathway, the superexchange through the Cr-O-Cr ($\angle \text{Cr-O-Cr} = 127.6^\circ$) should contribute AF interactions according to GK rules [8, 15]. The reported FM contribution from the t_{2g} - e_g (t-e) hybridization on the Cr^{III} -O- Cr^{III} couplings via the virtual charge transfer (VCT) of t_{2g}^3 -O- e_g^0 is much weaker compared to the AF interaction in bulk RECrO_3 crystal [9]. As such, J_2 should exhibit a AF nature, or at least not FM-dominated nature. We attribute this strong FM nature to the more distorted molecular structure compared to its bulk crystal, which can induce much larger tilting in the Cr-O octahedron and lead to much stronger t-e hybridization. This assessment is further confirmed by quantitatively evaluating the competing mechanisms between AF and FM in J_2 , as shown next.

In the framework of t-e hybridization, the superexchange interactions of Cr^{III} ions include two parts: the superexchange interactions over the half-filled π bond

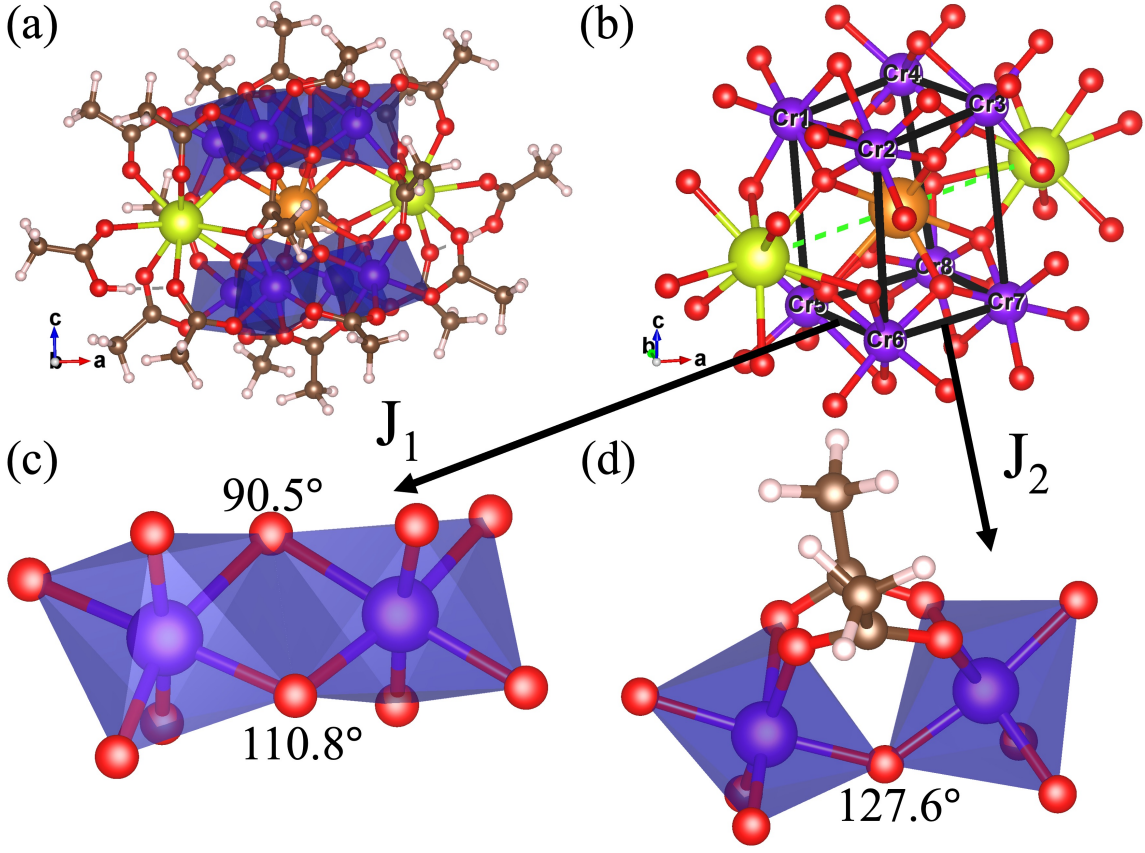


FIG. 1. The optimized molecular structure of Ce_3Cr_8 . (a) The complete molecular structure of Ce_3Cr_8 with $-CH_3$ as the ligand group. The CrO_6 octahedra are shaded in blue. Color scheme: Ce^{IV} orange; Ce^{III} green; Cr^{III} purple; O red. (b) The partially Ce_3Cr_8 central fragment without ligands, showing only the Ce-O and Cr-O bonds. The Ce line is denoted by a dotted line. The Cr curb is labelled by black line. (c) The detailed structure of J_1 (d)The detailed structure of J_2 , The average degrees of $\angle Cr-O-Cr$ are labeled in fig.

$t_{2g}^3-O-t_{2g}^3$, which is AF according to GK rules; the interaction between the half-filled π bond and empty σ bond, i.e., $t_{2g}^3-O-e_g^0$, due to the introduction of a VCT to the empty σ bond from t-e hybridization, which shows the FM coupling (see Supplementary materials section II and Fig. S2 for detailed information and the corresponding schematic hybridization diagram). The sum of this two parts gives the total interaction J in the J_2 path, as shown below[9],

$$J = J^\sigma - J^\pi \quad (2)$$

where J^π expresses the AF interaction via the VCT of $t_{2g}^3-O-t_{2g}^3$ and the J_{hb}^σ denotes FM interaction via the VCT of $t_{2g}^3-O-e_g^0$ due to t-e hybridization. They can be further expressed in an analytical form by considering all possible orbital overlap integrations between O and Cr [9] (also see Supplementary section II for detailed derivation), as shown below,

$$J = J_0[\eta(c^\sigma)^2 - (c^\pi)^2] \quad (3)$$

$$J_0 = \frac{(V_{pd}^\pi)^2}{U + \Delta_{ex}} \quad (4)$$

$$\eta = \frac{(V_{pd}^\sigma)^2}{(V_{pd}^\pi)^2} \cdot \frac{U + \Delta_{ex}}{U + \Delta_c} \quad (5)$$

$$c^\sigma = [\cos\left(\frac{w}{2}\right) + \sin\left(\frac{w}{2}\right)] \left\{ \sqrt{3} \cos\left(\frac{w}{2}\right) \sin\left(\frac{w}{2}\right) + \frac{\sqrt{3}}{2} [\cos^2\left(\frac{w}{2}\right) - \sin^2\left(\frac{w}{2}\right)] - \frac{1}{2} \right\} \quad (6)$$

$$c^\pi = 2 \left[\sin\left(\frac{w}{2}\right) + \cos\left(\frac{w}{2}\right) \right] - 4 \sin\left(\frac{w}{2}\right) \cos^2\left(\frac{w}{2}\right) \quad (7)$$

where J_0 is a prefactor depending on orbital overlap integral V_{pd}^π , the on-site Coulomb U and the exchange splitting Δ_{ex} ; η is a dimensionless parameter defined as the multiplication of two ratios, an orbital overlap integral ratio $\left(\frac{V_{pd}^\sigma}{V_{pd}^\pi}\right)^2$ and an energy ratio $\left(\frac{U + \Delta_{ex}}{U + \Delta_c}\right)$. Δ_c is the

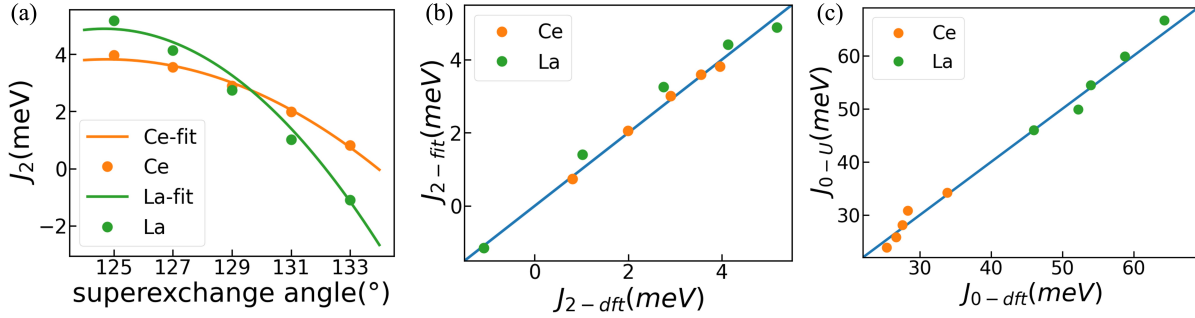


FIG. 2. Plot of superexchange strength from DFT calculated and model fitted values in Ce_3Cr_8 and $[\text{La}_3\text{Cr}_8]^{-1}$. (a) J_2 from DFT versus the superexchange angle Cr-O-Cr; (b) J_2 from model fitted values according to Eq. 3 ($J_2 - fit$) versus DFT calculated values ($J_2 - dft$); (c) J_0 calculated from Eq. 4 ($J_0 - U$) versus fitted from DFT results according to Eq. 3 ($J_0 - dft$).

crystal-field splitting; c^π and c^σ are parameters evolving with the bridging angle of $\angle\text{Cr-O-Cr}$ (w) [8, 9, 36]. In order to quantitatively determine the origin of FM in Ce_3Cr_8 , we calculated a series of J_2 values (see Table I) by computing the total energies of the eight magnetic states at different cases (see Supplementary materials Table. S2 for the detailed results at each case), including 1) Ce_3Cr_8 molecule with different angles of $\angle\text{Cr-O-Cr}$ in J_2 ($125^\circ, 127^\circ, 129^\circ, 131^\circ, 133^\circ$); 2) $[\text{La}_3\text{Cr}_8]^{-1}$ molecule with different angles of $\angle\text{Cr-O-Cr}$ in J_2 ($125^\circ, 127^\circ, 129^\circ, 131^\circ, 133^\circ$). The $[\text{La}_3\text{Cr}_8]^{-1}$ molecule is obtained by replacing the three Ce ions with La ions and adding an additional electron to keep the valence state of Cr ions unchanged. The chosen of $[\text{La}_3\text{Cr}_8]^{-1}$ is stimulated by our previous work[15] showing that the unoccupied Ce^{IV} - f orbital can enhance the FM interaction between transition metals after comparing the exchange coupling strengths between $[\text{Ce}_3\text{TM}_8]$ and $[\text{La}_3\text{TM}_8]^{-1}$.

With the data of angle dependent J_2 in Table I, we then fit Eq 3 by setting J_2 (J in Eq. 3) as the y values, angle (w) as the x values, and J_0 and η as the fitting parameters. An excellent fit was obtained by observing the fitted curves as well as the corresponding parity plot (see Fig. 2a, b). This clearly indicates the validity of Eq. 3 in describing the exchange mechanisms in Ce_3Cr_8 and La_3Cr_8 . The fitted parameters for J_0 and η are 26.63 meV, 1.86 and 52.22 meV, 1.81 for Ce_3Cr_8 and La_3Cr_8 , respectively. The J_0 for Ce_3Cr_8 is about half of that in La_3Cr_8 , while η is almost unchanged, whose value is also reasonable[9]. The value of J_0 determines the sensitivity of the change of J_2 with respect to the superexchange angle TM-O-TM. With the increase of the TM-O-TM angle, the exchange coupling can eventually turn to AF dominated, e.g. the studied superexchange J_2 (see Table. I). Thus the exchange coupling in Ce_3Cr_8 does not always show more FM nature than that in La_3Cr_8 , which is different from Ce_3Mn_8 [15] or Ce_3Fe_8 [16]. The validity of Eq. 4 is further demonstrated with the following steps: 1) Selecting a series of U values (1.5 eV, 2.0 eV, 2.5 eV, 3.0 eV, 3.5 eV) and at each U value, calculate angle-dependent J_2 values (see Supplementary material Table S3 and Table S4 for the detailed calculation data)

and fit Eq. 3 to obtain the fitted J_0 for each U value; 2) Estimate Δ_{ex} by constructing the maximally localized Wannier functions (MLWFs) based on the ferromagnetic electronic structure[37]. Our estimated values of Δ_{ex} are 4.3 eV and 4.2 eV for Ce_3Cr_8 and La_3Cr_8 when $U = 3.0$ eV, respectively. The change of Δ_{ex} is about one fifth of the change of U values, e.g., $\Delta_{ex1} - \Delta_{ex2} = 1/5(U_1 - U_2)$; 3) Fit Eq 4 by setting J_0 obtained from step 1 as the y values, U as the x values, and V_{pd}^π as the fitting parameters. The corresponding parity plot with a unity slope is shown in Fig 2(c) (see Supplementary materials Fig. S3 for the fitted curves), which indicates the effective of Eq. 4 in describing the U dependence of J_0 . Overall, the superexchange model in the framework of t-e hybridization can correctly describe our DFT calculated results in Re_3Cr_8 , confirming that the extraordinary FM dominated exchange coupling in the molecule is originated from the t-e hybridization, which is distinct with its bulk crystal due to the much larger distortion with even smaller TM-O-TM angle in the molecules.

To understand the reason why J_0 in Ce_3Cr_8 (26.63 meV) is much small compared to that in La_3Cr_8 (52.22 meV), which is responsible to the much less sensitivity of J_2 with respect to the TM-O-TM angles in Ce_3Cr_8 (orange curve in Fig. 2a) compared to that in La_3Cr_8 (green curve in Fig. 2a), we can reasonably attribute to the obvious difference between Ce_3Cr_8 and La_3Cr_8 , that at, the effect of the f orbitals. The projected density of state (PDOS) plots (see Fig. 3a, b) for FM state of both Ce_3Cr_8 and La_3Cr_8 show that Ce- f orbitals are much closer to the Fermi level compared to the La- f . A higher hybridization between Ce-4f and O-2p is also observed in Ce_3Cr_8 , e.g., the PDOS of Ce-4f orbitals and O-2p orbitals have similar peak in the same energy in Ce_3Cr_8 (see Fig. 3 c,d). The above evidence indicate that the VCT can happen in Ce-O but not in La-O. In addition, the fitted parameters V_{pd}^π in Eq. 4 are 0.42 eV and 0.60 eV for Ce_3Cr_8 and La_3Cr_8 , respectively. While the similar hopping terms calculated from WLWFs(see supplementary materials Table. S5) and the same form of overlap integral in the Slater's approach[36] indicate that the orbital overlap integral V_{pd}^π should be close with

each other in the two systems. This discrepancy also reminds us that a correction should be applied to the t-e hybridization framework to include the effects of f orbitals.

To include the f orbitals in the process of VCT, we extend the t-e hybridization framework according to superexchange model[12–14, 36, 38](see supplementary materials section II for detailed analysis), as shown below,

$$J = J_d + J_f \quad (8)$$

$$J_d = \frac{(b_{pd}^\sigma)^2}{U + \Delta_c} - \frac{(b_{pd}^\pi)^2}{U + \Delta_{ex}} \quad (9)$$

$$J_f = 0.5 \left[\frac{(b_{pd}^\pi)^2}{U + \Delta_{ex}} - \frac{(b_{pd}^\sigma)^2}{U + \Delta_c} \right] - \frac{(b_{pf}^\sigma)^2}{U + \Delta_f} + \frac{(b_{pf}^\pi)^2}{U + \Delta_f} \quad (10)$$

$$b_{pd} = c_{pd} \cdot V_{pd}; b_{pf} = c_{pf} \cdot V_{pf} \quad (11)$$

$$J_{Ce} = J_d + J_f = 0.5 \left[\frac{(b_{pd\sigma}^{Ce})^2}{U + \Delta_c^{Ce}} - \frac{(b_{pd\pi}^{Ce})^2}{U + \Delta_{ex}^{Ce}} \right] \quad (12)$$

$$J_{La} = J_d = \frac{(b_{pd\sigma}^{La})^2}{U + \Delta_c^{La}} - \frac{(b_{pd\pi}^{La})^2}{U + \Delta_{ex}^{La}} \quad (13)$$

$$J_0^{La} = \frac{(V_{pd\pi}^{La})^2}{U + \Delta_{ex}^{La}}; J_0^{Ce} = \frac{0.5(V_{pd\pi}^{Ce})^2}{U + \Delta_{ex}^{Ce}} \quad (14)$$

where J_d and J_f are the exchange coupling contribution from d orbitals and f orbitals, respectively. J_{Ce} and J_{La} are the exchange coupling contribution in Ce_3Cr_8 and La_3Cr_8 molecule, respectively. The different b variables are transfer integrals of corresponding orbitals (see supplementary materials Section II for detailed formula). Eq. 9 is the same with Eq. 3 with integrating the dimensionless c parameters to the transfer integrals b , as shown in Eq. Eq. 11. For J_f in Eq. 10, the Ce-O bonds are approximately perpendicular to the J_2 path (the degree of $\angle Cr-O-Ce$ is close to 90°) (see Fig 3 e-f), thus the symmetry in the Ce-O-Cr bonds are opposite to that in the Cr-O-Cr bonds, that is σ and π in Cr-O-Cr should be π and σ in Cr-O-Ce. To keep consistent notation of σ and π , an opposite sign of $\frac{(b_{pd}^\pi)^2}{U + \Delta_{ex}}$ and $\frac{(b_{pd}^\sigma)^2}{U + \Delta_c}$ is assigned in J_f in Eq. 10 compared to J_d in Eq. 9[14]. The Cr-O-Cr path has two $O^{2-}-Cr^{3+}$ exchange coupling interactions, while the Cr-O-Ce path only has one $O^{2-}-Cr^{3+}$ exchange coupling according to Anderson's mechanism[38]. This leads to the prefactor of pd superexchange coupling in J_f is half of that in J_d . The b_{pf} contributions from the VCT to unoccupied 4f orbitals in La_3Cr_8 can be ignored due to the negligible exchange interaction from the La-f

orbitals, as discussed in the previous paragraph. However, even in Ce_3Cr_8 , the b_{pf} is still an order of magnitude smaller than b_{pd} (see supplementary materials Table. S6). Therefore, the J_0 in Ce_3Cr_8 and La_3Cr_8 can be finally expressed in the form of Eq. 14, which clearly indicates that J_0 in Ce_3Cr_8 (26.63 meV) is about half of that in La_3Cr_8 (52.22 meV) after considering the effects of f orbitals. Noting that $\frac{(V_{pd\pi})^2}{U + \Delta_{ex}}$ in Ce_3Cr_8 and La_3Cr_8 are approximately the same.

TABLE I. The exchange coupling parameters (J) in meV of Ce_3Cr_8 and La_3Cr_8 . The degree of the $\angle Cr-O-Cr$ in J_2 is labeled. The difference of the parameters in La_3Cr_8 with respect to those in Ce_3Cr_8 are shown in parentheses.

J Path	Ce_3Cr_8	La_3Cr_8
J_1 (relaxed structure)	1.09	1.54 (+0.45)
J_2 (relaxed structure)	2.17	2.53 (+0.36)
125- J_2	3.96	5.17 (+1.21)
127- J_2	3.55	4.13 (+0.58)
129- J_2	2.90	2.75 (-0.15)
131- J_2	1.99	1.02 (-0.97)
133- J_2	0.81	-1.09 (-1.90)

Discussion.—We have theoretically investigated the atomic structure, electronic and magnetic properties of the molecule analogue of perovskite chromites, abbreviated as Ce_3Cr_8 , using the first-principles method. In particular, we found a unexpected dominate FM interaction in magnetic coupling between two NN Cr sites with angle Cr-O-Cr much greater than 90° , distinct from the bulk perovskite chromites[8, 9]. The magnetic coupling between Cr ions evolving with the degree of $\angle Cr-O-Cr$ follows the t-e hybridization framework, confirming that the dominated FM nature is originated from t-e hybridization. In particular, due to the great sensitivity of t-e hybridization with respect to the superexchange angle Cr-O-Cr, little molecular structure change can induce significant difference in the magnetic exchange coupling strength with the ground state evolving a transition from FM to AF. This structure-dependent magnetic interaction mechanism can be applied to develop multifunctional molecule-based magnetic devices.

The effects of the Re- f orbitals to the exchange interaction of TM ions was initially pointed out in Ce_3Mn_8 by contributing a direct FM interaction[15], which was also confirmed in Ce_3Fe_8 [16]. Our calculation results in Ce_3Cr_8 also indicate that the Ce- f orbitals can place effects on the superexchange interaction between TM ions but with a different mechanism from the previous work. In Fig 2c, we can find that Ce- f orbitals can significantly change the sensitivity of J_2 with respect to the structure change, not just contributing FM or AF interaction. All the works on the analysis of the effects of f orbitals show that only the orbitals near the Fermi level can have sizable contribution to the superexchange interaction. Hence the effects of f orbitals on the t-e hybridization are closely related to the energy level po-

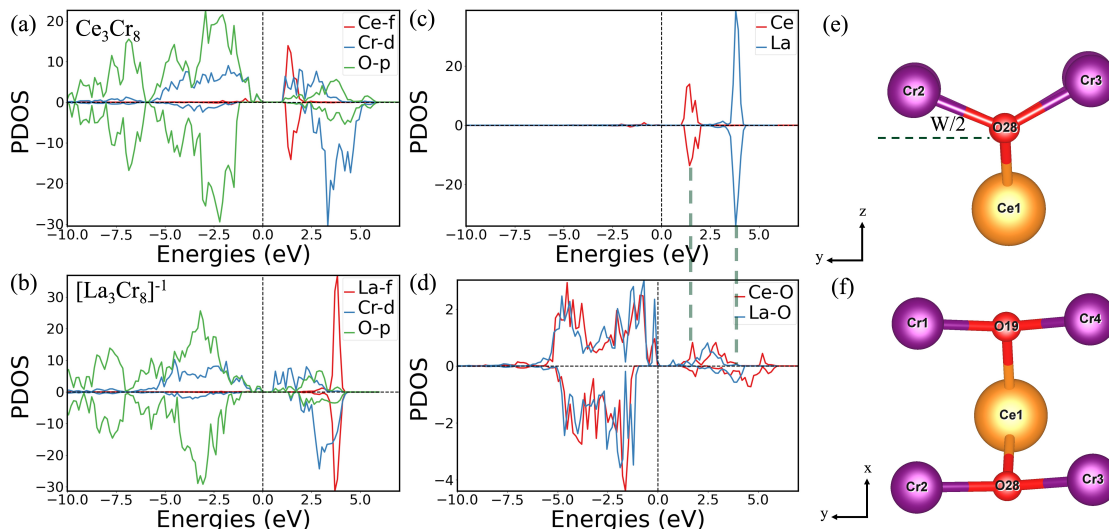


FIG. 3. The projected density of states (PDOS) for (a) FM(ground state) of Ce_3Fe_8 and (b) $[\text{La}_3\text{Fe}_8]^{-1}$ (c) Ce-f and La-f orbitals in Ce_3Cr_8 and La_3Cr_8 (d) O-p of J_2 in Ce_3Cr_8 and La_3Cr_8 . The PDOS plots are corresponding orbital-resolved, respectively. (e,f) Schematic diagram of J_2 structure.

sition of the orbitals, which can be modulated by the type of cations and TM elements, as well as the molecular geometry. For example, charging the molecule can significantly change the molecular geometries and energy levels of the orbitals [17, 39], thus in turn to modify the magnetic interactions within the molecules.

Conclusion.—In conclusion, our investigation of the Ce_3Cr_8 magnetic molecule elaborates the complex magnetism involving both t-e hybridization and Re-f orbitals at the nanoscale. The superexchange via the Cr-d and O-p orbitals can provide a dominate FM interaction for both J_1 and J_2 through strong t-e hybridization induced by the structure distortion. The superexchange interaction involving the t-e hybridization is very sensitive to the molecular structure, e.g. the ground state can undergo a FM to AFM transition upon the structural change, which

can be further modulated by the Re-f orbitals. In particular, the inclusion of Ce-f orbitals can decrease the sensitivity of the change of the magnetic coupling with respect to the molecular structural changes. Our theoretical work complements the theory of superexchange magnetism involving t-e hybridization and adds another dimension to fine tune the magnetic properties of nanoscale molecules through Tm-d/Re-f interactions.

ACKNOWLEDGMENTS

The authors would like to acknowledge financial support from the Hundreds of Talents Program of Sun Yat-sen University.

-
- [1] A. Narayan, A. Cano, A. V. Balatsky, and N. A. Spaldin, Multiferoic quantum criticality, *Nature materials* **18**, 223 (2019).
 - [2] C. Wang, L. You, D. Cobden, and J. Wang, Towards two-dimensional van der waals ferroelectrics, *Nature Materials*, 1 (2023).
 - [3] A. G. Ricciardulli, S. Yang, J. H. Smet, and M. Saliba, Emerging perovskite monolayers, *Nature Materials* **20**, 1325 (2021).
 - [4] N. A. Spaldin and R. Ramesh, Advances in magnetoelectric multiferroics, *Nature materials* **18**, 203 (2019).
 - [5] X. Wang, Y. Chai, L. Zhou, H. Cao, C.-d. Cruz, J. Yang, J. Dai, Y. Yin, Z. Yuan, S. Zhang, *et al.*, Observation of magnetoelectric multiferroicity in a cubic perovskite system: $\text{LaMn}_3\text{Cr}_4\text{O}_{12}$, *Physical review letters* **115**, 087601 (2015).
 - [6] W. Li, Z. Wang, F. Deschler, S. Gao, R. H. Friend, and A. K. Cheetham, Chemically diverse and multifunctional hybrid organic-inorganic perovskites, *Nature Reviews Materials* **2**, 1 (2017).
 - [7] H. Schmid, Multi-ferroic magnetoelectrics, *Ferroelectrics* **162**, 317 (1994).
 - [8] Y. Zhu, J. Xia, S. Wu, K. Sun, Y. Yang, Y. Zhao, H. W. Kan, Y. Zhang, L. Wang, H. Wang, *et al.*, Crystal growth engineering and origin of the weak ferromagnetism in antiferromagnetic matrix of orthochromates from te orbital hybridization, *Iscience* **25** (2022).
 - [9] J.-S. Zhou, J. Alonso, V. Pomjakushin, J. B. Goodenough, Y. Ren, J.-Q. Yan, and J.-G. Cheng, Intrinsic structural distortion and superexchange interaction in the orthorhombic rare-earth perovskites RCrO_3 , *Physical Review B* **81**, 214115 (2010).

- [10] J.-S. Zhou, J. Alonso, A. Muoz, M. Fernández-Díaz, and J. Goodenough, Magnetic structure of LaCoO_3 perovskite under high pressure from in situ neutron diffraction, *Physical Review Letters* **106**, 057201 (2011).
- [11] E. Moon, Q. He, S. Ghosh, B. Kirby, S. Pantelides, A. Borisevich, and S. May, Structural “ δ doping” to control local magnetization in isovalent oxide heterostructures, *Physical Review Letters* **119**, 197204 (2017).
- [12] J. B. Goodenough, Theory of the role of covalence in the perovskite-type manganites [la, m (ii)] mn o 3, *Physical Review* **100**, 564 (1955).
- [13] J. B. Goodenough, An interpretation of the magnetic properties of the perovskite-type mixed crystals $\text{La}_{1-x}\text{Sr}_x\text{CoO}_3$ - λ , *Journal of Physics and Chemistry of Solids* **6**, 287 (1958).
- [14] J. Kanamori, Superexchange interaction and symmetry properties of electron orbitals, *Journal of Physics and Chemistry of Solids* **10**, 87 (1959).
- [15] A. E. Thuijs, X.-G. Li, Y.-P. Wang, K. A. Abboud, X.-G. Zhang, H.-P. Cheng, and G. Christou, Molecular analogue of the perovskite repeating unit and evidence for direct $\text{M}^{\text{III}}\text{-O}-\text{M}^{\text{III}}$ exchange coupling pathway, *Nature communications* **8**, 500 (2017).
- [16] M. Wang, T. Wang, M. Yuan, Q. Zhang, S. Liu, J. Shuai, and X.-G. Li, Molecular analog of perovskite ferrites: First-principles studies of electronic and magnetic properties, *Physical Review B* **108**, 184421 (2023).
- [17] Y.-P. Wang, X.-G. Li, X.-G. Zhang, G. Christou, and H.-P. Cheng, Cation substitution effect on a molecular analogue of perovskite manganites, *The Journal of Physical Chemistry C* **121**, 10893 (2017).
- [18] W. Kohn and L. J. Sham, Self-consistent equations including exchange and correlation effects, *Physical review* **140**, A1133 (1965).
- [19] J. P. Perdew, K. Burke, and M. Ernzerhof, Generalized gradient approximation made simple, *Physical review letters* **77**, 3865 (1996).
- [20] G. Kresse and J. Furthmüller, Efficiency of ab-initio total energy calculations for metals and semiconductors using a plane-wave basis set, *Computational materials science* **6**, 15 (1996).
- [21] G. Kresse and J. Furthmüller, Efficient iterative schemes for ab initio total-energy calculations using a plane-wave basis set, *Physical review B* **54**, 11169 (1996).
- [22] P. E. Blöchl, Projector augmented-wave method, *Physical review B* **50**, 17953 (1994).
- [23] G. Kresse and D. Joubert, From ultrasoft pseudopotentials to the projector augmented-wave method, *Physical review b* **59**, 1758 (1999).
- [24] C. Loschen, J. Carrasco, K. M. Neyman, and F. Illas, First-principles $\text{LDA}+u$ and $\text{GGA}+u$ study of cerium oxides: Dependence on the effective u parameter, *Physical Review B* **75**, 035115 (2007).
- [25] J. Hong, A. Stroppa, J. Íñiguez, S. Picozzi, and D. Vanderbilt, Spin-phonon coupling effects in transition-metal perovskites: A $\text{dft}+u$ and hybrid-functional study, *Physical Review B* **85**, 054417 (2012).
- [26] A. A. Mostofi, J. R. Yates, Y.-S. Lee, I. Souza, D. Vanderbilt, and N. Marzari, wannier90: A tool for obtaining maximally-localised wannier functions, *Computer physics communications* **178**, 685 (2008).
- [27] J. Zhang, C. Ji, J. Wang, W. Xia, X. Lu, and J. Zhu, Stabilization of e-type magnetic order caused by epitaxial strain in perovskite manganites, *Physical Review B* **97**, 085124 (2018).
- [28] A. Shorikov, A. Lukoyanov, M. Korotin, and V. Anisimov, Magnetic state and electronic structure of the δ and α phases of metallic Pu and its compounds, *Physical Review B* **72**, 024458 (2005).
- [29] I. Shein, K. Shein, V. Kozhevnikov, and A. Ivanovskii, Band structure and the magnetic and elastic properties of SrFeO_3 and LaFeO_3 perovskites, *Physics of the Solid State* **47**, 2082 (2005).
- [30] A. Abbad, W. Benstaali, H. Bentounes, S. Bentata, and Y. Benmalem, Search for half-metallic ferromagnetism in orthorhombic $\text{Ce}(\text{Fe/Cr})\text{O}_3$ perovskites, *solid state communications* **228**, 36 (2016).
- [31] L. Noodleman, Valence bond description of antiferromagnetic coupling in transition metal dimers, *The Journal of Chemical Physics* **74**, 5737 (1981).
- [32] L. Noodleman and E. R. Davidson, Ligand spin polarization and antiferromagnetic coupling in transition metal dimers, *Chemical physics* **109**, 131 (1986).
- [33] L. Noodleman, C. Peng, D. Case, and J.-M. Mouesca, Orbital interactions, electron delocalization and spin coupling in iron-sulfur clusters, *Coordination Chemistry Reviews* **144**, 199 (1995).
- [34] K. Yamaguchi, T. Tsunekawa, Y. Toyoda, and T. Fueno, Ab initio molecular orbital calculations of effective exchange integrals between transition metal ions, *Chemical physics letters* **143**, 371 (1988).
- [35] K. Yamaguchi, T. Fueno, N. Ueyama, A. Nakamura, and M. Ozaki, Antiferromagnetic spin couplings between iron ions in iron—sulfur clusters. a localized picture by the spin vector model, *Chemical physics letters* **164**, 210 (1989).
- [36] J. C. Slater and G. F. Koster, Simplified LCAO method for the periodic potential problem, *Physical review* **94**, 1498 (1954).
- [37] K. Liu, Y. Hou, X. Gong, and H. Xiang, Orbital delocalization and enhancement of magnetic interactions in perovskite oxyhydrides, *Scientific Reports* **6**, 19653 (2016).
- [38] P. W. Anderson, New approach to the theory of superexchange interactions, *Physical Review* **115**, 2 (1959).
- [39] X.-G. Li, X.-G. Zhang, and H.-P. Cheng, Conformational electroresistance and hysteresis in nanoclusters, *Nano letters* **14**, 4476 (2014).
- [1] A. Narayan, A. Cano, A. V. Balatsky, and N. A. Spaldin, Multiferroic quantum criticality, *Nature materials* **18**, 223 (2019).
- [2] C. Wang, L. You, D. Cobden, and J. Wang, Towards two-dimensional van der waals ferroelectrics, *Nature Materials*, 1 (2023).
- [3] A. G. Ricciardulli, S. Yang, J. H. Smet, and M. Saliba, Emerging perovskite monolayers, *Nature Materials* **20**, 1325 (2021).
- [4] N. A. Spaldin and R. Ramesh, *Advances in magnetoelectrics*, 1 (2023).

- tric multiferroics, *Nature materials* **18**, 203 (2019).
- [5] X. Wang, Y. Chai, L. Zhou, H. Cao, C.-d. Cruz, J. Yang, J. Dai, Y. Yin, Z. Yuan, S. Zhang, *et al.*, Observation of magnetoelectric multiferroicity in a cubic perovskite system: $\text{LaMn}_3\text{Cr}_4\text{O}_{12}$, *Physical review letters* **115**, 087601 (2015).
- [6] W. Li, Z. Wang, F. Deschler, S. Gao, R. H. Friend, and A. K. Cheetham, Chemically diverse and multifunctional hybrid organic–inorganic perovskites, *Nature Reviews Materials* **2**, 1 (2017).
- [7] H. Schmid, Multi-ferroic magnetoelectrics, *Ferroelectrics* **162**, 317 (1994).
- [8] Y. Zhu, J. Xia, S. Wu, K. Sun, Y. Yang, Y. Zhao, H. W. Kan, Y. Zhang, L. Wang, H. Wang, *et al.*, Crystal growth engineering and origin of the weak ferromagnetism in antiferromagnetic matrix of orthochromates from the orbital hybridization, *Iscience* **25** (2022).
- [9] J.-S. Zhou, J. Alonso, V. Pomjakushin, J. B. Goodenough, Y. Ren, J.-Q. Yan, and J.-G. Cheng, Intrinsic structural distortion and superexchange interaction in the orthorhombic rare-earth perovskites R_2CrO_3 , *Physical Review B* **81**, 214115 (2010).
- [10] J.-S. Zhou, J. Alonso, A. Muoz, M. Fernández-Díaz, and J. Goodenough, Magnetic structure of LaCrO_3 perovskite under high pressure from *in situ* neutron diffraction, *Physical Review Letters* **106**, 057201 (2011).
- [11] E. Moon, Q. He, S. Ghosh, B. Kirby, S. Pantelides, A. Borisevich, and S. May, Structural “ δ doping” to control local magnetization in isovalent oxide heterostructures, *Physical Review Letters* **119**, 197204 (2017).
- [12] J. B. Goodenough, Theory of the role of covalence in the perovskite-type manganites [la, m (ii)] MnO_3 , *Physical Review* **100**, 564 (1955).
- [13] J. B. Goodenough, An interpretation of the magnetic properties of the perovskite-type mixed crystals $\text{La}_{1-x}\text{Sr}_x\text{CoO}_3$, *Journal of Physics and Chemistry of Solids* **6**, 287 (1958).
- [14] J. Kanamori, Superexchange interaction and symmetry properties of electron orbitals, *Journal of Physics and Chemistry of Solids* **10**, 87 (1959).
- [15] A. E. Thuijs, X.-G. Li, Y.-P. Wang, K. A. Abboud, X.-G. Zhang, H.-P. Cheng, and G. Christou, Molecular analogue of the perovskite repeating unit and evidence for direct $\text{Mn}^{III}\text{-O-Mn}^{III}$ exchange coupling pathway, *Nature communications* **8**, 500 (2017).
- [16] M. Wang, T. Wang, M. Yuan, Q. Zhang, S. Liu, J. Shuai, and X.-G. Li, Molecular analog of perovskite ferrites: First-principles studies of electronic and magnetic properties, *Physical Review B* **108**, 184421 (2023).
- [17] Y.-P. Wang, X.-G. Li, X.-G. Zhang, G. Christou, and H.-P. Cheng, Cation substitution effect on a molecular analogue of perovskite manganites, *The Journal of Physical Chemistry C* **121**, 10893 (2017).
- [18] W. Kohn and L. J. Sham, Self-consistent equations including exchange and correlation effects, *Physical review* **140**, A1133 (1965).
- [19] J. P. Perdew, K. Burke, and M. Ernzerhof, Generalized gradient approximation made simple, *Physical review letters* **77**, 3865 (1996).
- [20] G. Kresse and J. Furthmüller, Efficiency of *ab-initio* total energy calculations for metals and semiconductors using a plane-wave basis set, *Computational materials science* **6**, 15 (1996).
- [21] G. Kresse and J. Furthmüller, Efficient iterative schemes for *ab initio* total-energy calculations using a plane-wave basis set, *Physical review B* **54**, 11169 (1996).
- [22] P. E. Blöchl, Projector augmented-wave method, *Physical review B* **50**, 17953 (1994).
- [23] G. Kresse and D. Joubert, From ultrasoft pseudopotentials to the projector augmented-wave method, *Physical review b* **59**, 1758 (1999).
- [24] C. Loschen, J. Carrasco, K. M. Neyman, and F. Illas, First-principles $\text{LDA}+u$ and $\text{GGA}+u$ study of cerium oxides: Dependence on the effective u parameter, *Physical Review B* **75**, 035115 (2007).
- [25] J. Hong, A. Stroppa, J. Íñiguez, S. Picozzi, and D. Vanderbilt, Spin-phonon coupling effects in transition-metal perovskites: A $\text{DFT}+u$ and hybrid-functional study, *Physical Review B* **85**, 054417 (2012).
- [26] A. A. Mostofi, J. R. Yates, Y.-S. Lee, I. Souza, D. Vanderbilt, and N. Marzari, wannier90: A tool for obtaining maximally-localised wannier functions, *Computer physics communications* **178**, 685 (2008).
- [27] J. Zhang, C. Ji, J. Wang, W. Xia, X. Lu, and J. Zhu, Stabilization of e -type magnetic order caused by epitaxial strain in perovskite manganites, *Physical Review B* **97**, 085124 (2018).
- [28] A. Shorikov, A. Lukoyanov, M. Korotin, and V. Anisimov, Magnetic state and electronic structure of the δ and α phases of metallic Pu and its compounds, *Physical Review B* **72**, 024458 (2005).
- [29] I. Shein, K. Shein, V. Kozhevnikov, and A. Ivanovskii, Band structure and the magnetic and elastic properties of SrFeO_3 and LaFeO_3 perovskites, *Physics of the Solid State* **47**, 2082 (2005).
- [30] A. Abbad, W. Benstaali, H. Bentounes, S. Bentata, and Y. Benmalem, Search for half-metallic ferromagnetism in orthorhombic $\text{Ce}(\text{Fe}/\text{Cr})\text{O}_3$ perovskites, *solid state communications* **228**, 36 (2016).
- [31] L. Noodleman, Valence bond description of antiferromagnetic coupling in transition metal dimers, *The Journal of Chemical Physics* **74**, 5737 (1981).
- [32] L. Noodleman and E. R. Davidson, Ligand spin polarization and antiferromagnetic coupling in transition metal dimers, *Chemical physics* **109**, 131 (1986).
- [33] L. Noodleman, C. Peng, D. Case, and J.-M. Mouesca, Orbital interactions, electron delocalization and spin coupling in iron-sulfur clusters, *Coordination Chemistry Reviews* **144**, 199 (1995).
- [34] K. Yamaguchi, T. Tsunekawa, Y. Toyoda, and T. Fueno, *Ab initio* molecular orbital calculations of effective exchange integrals between transition metal ions, *Chemical physics letters* **143**, 371 (1988).
- [35] K. Yamaguchi, T. Fueno, N. Ueyama, A. Nakamura, and M. Ozaki, Antiferromagnetic spin couplings between iron ions in iron–sulfur clusters. a localized picture by the spin vector model, *Chemical physics letters* **164**, 210 (1989).
- [36] J. C. Slater and G. F. Koster, Simplified LCAO method for the periodic potential problem, *Physical review* **94**, 1498 (1954).
- [37] K. Liu, Y. Hou, X. Gong, and H. Xiang, Orbital delocalization and enhancement of magnetic interactions in perovskite oxyhydrides, *Scientific Reports* **6**, 19653 (2016).
- [38] P. W. Anderson, New approach to the theory of superexchange interactions, *Physical Review* **115**, 2 (1959).
- [39] X.-G. Li, X.-G. Zhang, and H.-P. Cheng, Conformational

electroresistance and hysteresis in nanoclusters, Nano letters **14**, 4476 (2014).